Interaction between the AAA+ ATPase p97 and its Cofactor Ataxin3 in Health and Disease: Nucleotide-induced Conformations Regulate Cofactor Binding.

Maya V. Rao[‡], Dewight R. Williams[§], Simon Cocklin[‡], and Patrick J. Loll[‡]

From the [‡]Department of Biochemistry and Molecular Biology, Drexel University College of Medicine, Philadelphia, PA 19102, USA and
[§]LeRoy Eyring Center for Solid State Science, Arizona State University, Tempe, AZ 85287, USA

SUPPLEMENTAL DATA *(List of Contents)*

- Protein Expression and Purification
- Surface Plasmon Resonance
- Table S1: *Expression constructs used and primers used to generate them.*
- Table S2: *Primers used for one-step site-directed mutagenesis.*
- Figure S1: *Alternate p97 preparations have the same affinity for ataxin3.*
- Figure S2: *Negative-stain EM analyses of the p97-ataxin3 complex.*
- Figure S3: *Comparison of non-crosslinked and crosslinked samples for EM.*
- Figure S4: *SDS-PAGE gel of the crosslinked and non-crosslinked EM complexes.*
- Figure S5: *p97 complexed with Nanogold-labeled ataxin3.*
- Figure S6: *ATPase activities of p97 – wild-type, binding-cleft mutants, and Walker mutants.*
- Figure S7: *ATPase activities of p97 – wild-type and MSP1 mutants.*
- Figure S8: *ATPase activities of p97 – wild-type and mutants, with and without DTT.*
- Figure S9: *Ataxin3ΔC binds a conformationally-locked form of p97, unlike full-length ataxin3.*
- Figure S10: *Ataxin3 binds MSP1 versions of the R155C/N387C double mutant.*
- Figure S11: *Elution profile of full-length p97 from size-exclusion chromatography.*
- Figure S12: *Global 1:1 kinetic analysis of full-length ataxin3 binding to full-length p97.*
- Figure S13: *Detecting the presence of mass-transport limitations in the p97-ataxin3 system.*
- Table S3: *Binding affinities and structures for various p97-cofactor complexes.*

SUPPLEMENTAL DATA

Protein Expression and Purification

All proteins were expressed in *E. coli* Rosetta (DE3) cells (Novagen), by induction with 1 mM isopropyl-β-D-thiogalactopyranoside (IPTG) at an A_{600} of 0.5–0.8, followed by shaking overnight at 24 °C. After roughly 21 h, the cells were harvested by centrifugation at 5,000 × *g* and the pellets were resuspended in water and flash-frozen. Attempts were made to express the p97 N-domain in *E. coli* Rosetta (DE3) cells using an auto-induction protocol (1), but this resulted in a large amount of the protein being in the pellet after the centrifugation steps, indicating denatured or aggregated protein; this was not observed when using the IPTG induction protocol. Preceding purification, the pellets were rapidly thawed under running water and resuspended in lysis buffer. All cells were lysed by at least two passes through a chilled Emulsiflex-C5 homogenizer (Avestin, Ontario, Canada) at approximately 173 MPa. For the His_6-SUMO-fusions, lysis, clarification and subtractive purification were performed as described previously (2), expect for minor changes described below.

For all the His_6-SUMO-ataxin3 constructs (full-length wild-type, full-length 282ANAA285 mutant, Josephin domain, Josephin + UIMs, ataxin3ΔC and ataxin3ΔN), the cells were lysed in 50 mM sodium phosphate, pH 8.0, 250 mM NaCl, 20 mM imidazole, 10 mM $MgCl_2$, 5 mM β-mercaptoethanol (βME), 5% v/v glycerol, 1 µg/ml each DNAse and RNAse, and protease inhibitor (Prod. #88266, Pierce ThermoFisher; 1 tablet/ 50 ml lysate). The lysates were clarified at 311,000 × *g* for 1 h and loaded onto a HiTrap IMAC HP column pre-equilibrated with 50 mM sodium phosphate, pH 8.0, 250 mM NaCl, 20 mM imidazole, 5% v/v glycerol, 5 mM βME, and eluted using a 20–300 mM gradient of imidazole. The eluted fractions were pooled and dialyzed back into 50 mM sodium phosphate, pH 8.0, 250 mM NaCl, 20 mM imidazole, 5% v/v glycerol, 5 mM βME, at 4 °C, in the presence of the doubly-tagged SUMO-specific protease Ud1 (dtUd1) (2). 200 µg of protease is sufficient to cleave the amount of fusion protein obtained from a 1-L culture. After an overnight dialysis, the sample was applied to the same metal affinity chromatography column to remove the His_6-SUMO tag and the dtUD1 enzyme. After subtractive purification, the ataxin3 constructs were further purified by ion exchange chromatography. The proteins were first dialyzed against 50 mM sodium phosphate, pH 8.0, 50 mM NaCl, then loaded onto a HiTrap Sepharose Q HP column and eluted using a 50–1000 mM gradient of NaCl. The desired fractions were pooled and further purified by size-exclusion chromatography (SEC) on a HiPrep Sephacryl S-300 HR column equilibrated in 25 mM Tris, pH 8.0, 200 mM KCl, 5 mM $MgCl_2$, 5 mM βME. For the N-terminally His_6-tagged ataxin3 protein, the Ud1 cleavage and subtractive purification steps were omitted.

For all the His_6-SUMO-p97 constructs (full-length wild-type protein, with and without the C-terminal 1D4-tag, p97 N-domain, p97N + D1-domains, and all p97 mutants), the cell pellets were lysed in in 50 mM Tris, pH 8.0, 250 mM KCl, 20 mM imidazole, 10 mM $MgCl_2$, 5 mM βME, 5% v/v glycerol, 1

μg/ml each DNAse and RNAse, and protease inhibitor tablets (details above). Clarification and subtractive purification were performed as described for the ataxin3 constructs, except the IMAC buffer contained 50 mM Tris, pH 8.0, 250 mM KCl, 20 mM imidazole, 5 mM $MgCl_2$, 5 mM βME, 5% v/v glycerol, and the elution was over a 20–300 mM gradient of imidazole. After subtractive purification, the proteins were directly purified by gel filtration as described above. For the ITC experiments, full-length p97 was subjected to an additional ion exchange chromatography step before SEC, through a HiTrap Sepharose Q HP column, using a buffer with 100 mM HEPES, pH 7.0, 50 mM NaCl, 5 mM βME, and a 50–500 mM linear NaCl gradient. This step was to ensure the removal of any aggregated material in order to concentrate full-length p97 sufficiently for ITC. The C-terminally His_6-tagged full-length p97 was expressed as a SUMO-fusion, which helped in expression and solubility. The SUMO was later removed by cleavage with dtUd1 as described above, and the sample was purified by gel filtration. On our preparative Sephacryl S-300 column, the elution profile for full-length p97 was similar to that described by Niwa *et al.* (3) using a Superose 6 column (supplemental Fig. S11*A*). Niwa *et al.* verified that their void peak contained irreversibly aggregated material, and the additional shoulder present in their trace contained dodecameric p97 with some aggregates. To further analyze the size-exclusion behavior of p97, we injected full-length p97 onto a Yarra SEC-3000 column (for improved separation of high molecular-weight species), and observed a smaller peak between the void peak and hexamer peak (supplemental Fig. S11*B*). This peak most likely contained higher-order oligomers and/or aggregates, and was in equilibrium with the hexamer species, since reinjection of the hexamer peak yielded the same three-peak elution profile (data not shown).

For all ataxin3 and p97 proteins, the final SEC fractions from the Sephacryl S-300 column were pooled and concentrated to 8–10 mg/ml using an Amicon stirred cell (Millipore), and then aliquoted, flash-frozen, and stored at –80 °C.

Surface Plasmon Resonance (SPR)

All SPR experiments were performed on a BioRad ProteOn XPR36 at 25 °C. The full-length p97 hexamer was captured as a ligand in an oriented manner employing two different strategies, A) the Rho1D4 epitope-antibody system (4,5) and B) histidine-tagged protein capture.

A) Rho1D4 epitope-antibody system. The Rho1D4 monoclonal antibody was immobilized on a ProteOn GLC sensor chip by amine coupling using 1× PBS pH 7.4 plus 0.005% Tween® 20 as the running buffer. The surface was first activated with a freshly prepared mixture of 1-ethyl-3-(3-dimethylaminopropyl) carbodiimide hydrochloride (EDC) and N-hydroxysulfosuccinimide (sulpho-NHS), (final concentrations 20 mM EDC : 5 mM sulpho-NHS), at a flow rate of 30 μl/min for 5 min. The 1D4 antibody was diluted in 10 mM sodium acetate, pH 5.5 (final concentration 0.1–0.5 mg/ml), and

immobilized to a density of ~3,500 response units (RU) on the activated surface, at a flow rate of 30 µl/min for 7 min. Excess activated groups were blocked with 1 M ethanolamine-HCl, pH 8.5 at a flow rate of 30 µl/min for 5 min. The surface was stabilized by at least three consecutive injections of regeneration solution (freshly prepared 10 mM NaOH and 1% *N*-octyl-β-D-glucopyranoside), each at a flow rate of 100 µl/min for 18 s. For each sensor chip, one of the lanes with the immobilized 1D4 antibody was maintained as the reference surface. The buffer was switched to 25 mM Tris, pH 8.0, 200 mM KCl, 5 mM $MgCl_2$, 0.1 mM TCEP, 0.005% Tween® 20. C-terminally 1D4-tagged full-length p97 and p97 mutants were diluted into this buffer (final concentration 5–50 µg/ml) and captured (100–150 RU) as ligands on the antibody-coated surfaces, at a flow rate of 50 µl/min for 30 s. Various concentrations of analytes, including ataxin3, the 282ANAA285 mutant, and fragments with and without nucleotides, were diluted in the Tris buffer and passed over the chip at 150 µl/min, for the maximum possible contact time of 163 s. Some experiments involving the p97 R155C/N387C variant also included either 7 mM DTT or no reducing agent, instead of TCEP, as indicated in the main text and figures. The surface was regenerated completely with three injections of freshly prepared regeneration solution, at 100 µl/min for 18 s, before the next round of 1D4-tagged ligand capture.

B) His_6-tagged protein capture. The ProteOn HTG sensor chip surface was first activated with 10 mM $NiSO_4$ (30 µl/min for 120 s) following the standard protocol recommended by the manufacturer. C-terminally His_6-tagged full-length p97 hexamer (final concentration 0.1–0.4 mg/ml) was captured on the chip to a density of 200–300 RU, using a flow rate of 30 µl/min for 120 s. A reference surface was generated for each chip using His_6-tagged MBP as a control protein. Full-length ataxin3 was flowed over as the analyte, at the concentrations indicated (supplemental Fig. S1), at 100 µl/min, for a contact time of 200 s. Running and dilution buffers used throughout contained 25 mM Tris, pH 8.0, 200 mM KCl, 5 mM $MgCl_2$, 1 mM βME, 5% v/v glycerol, and 0.005% Tween® 20, and the surface was regenerated with three injections of 300 mM EDTA, pH 8.5, at 30 µl/min for 800 s, before the next round of His_6-tagged p97 capture. We observed that a small amount of the ligand accumulated on the chip with each subsequent round of capture, presumably via non-specific aggregation, and the regeneration steps were thus unable to completely clear this material. However, reproducible results were obtained over as many as six rounds of p97-His_6 capture for each flow strip.

The p97 N-domain was immobilized as the ligand on a ProteOn GLC sensor chip by amine coupling, using the same protocol described above. 1D4-tagged N-domain was not used for SPR experiments, as baselines obtained with this construct displayed significant drift. The p97 N-domain was diluted in 10 mM sodium acetate, pH 5.0 (final concentration 20 µg/ml), and directly immobilized on an activated chip to a density of 400–500 RU, at 30 µl/min for 7 min. The chip was blocked with 1 M ethanolamine-HCl, pH 8.5 as described above and stabilized with at least three injections of running

buffer (30 µl/min for 1 min). The running and dilution buffers used for all p97 N-domain experiments contained 1× PBS, pH 7.4, and 0.005% Tween® 20. A reference surface was generated for each chip using the 1D4 antibody immobilized to the corresponding density. Full-length ataxin3 was flowed over as the analyte at the concentrations indicated (Fig. 2B), at 150 µl/min for a contact time of 163 s.

All binding data were first double-referenced to the control flow strip with immobilized Rho1D4 antibody alone, as well as buffer injections during the analyte step. The data were then normalized, relative to the total ligand density on the corresponding surface (Eq. 1), to account for minor differences in ligand immobilization between experiments.

$$Normalized\ analyte\ response\ = \frac{Observed\ analyte\ response}{Ligand\ density} \times 100 \qquad \text{Equation 1}$$

The processed data were fit to an equilibrium binding model using GraphPad Prism 7.0 to derive the binding affinity. A global 1:1 kinetic analysis of the binding data resulted in poor fits, especially at lower concentrations (supplemental Fig. S12). This deviation from ideal first-order binding kinetics may reflect the need for a more complex interaction model, or, alternatively, might indicate surface-induced artifacts. Since we had no substantial evidence to support a more complex interaction scheme (e.g., conformational changes occurring upon analyte binding or multiple binding sites), we probed the data for mass-transport effects and rebinding events, and optimized conditions to minimize these artifacts, following strategies recommended in (6). We first compared the initial association signals obtained by exposing analyte to different densities of the immobilized ligand (supplemental Fig. S13*A*). The analyte responses, when normalized to the total corresponding ligand density on that surface, produced superimposable curves across flow strips with densities < 200 RU. Ligand densities greater than 200 RU showed slower association kinetics, indicating the presence of mass transport artifacts (supplemental Fig. S13*A*). Thus, we ensured that p97-1D4 was captured to densities of 100–150 RU for all experiments; this level is low enough to minimize mass-transport effects and yet sufficiently high to maintain a good signal/noise ratio. Additionally, a high flow rate of 150 µl/min was used for the analyte, since we detected increased mass-transport effects using lower flow rates (data not shown). We also tested for rebinding events by introducing a competitor in the dissociation phase (excess untagged p97); by binding to the dissociated analyte, this competitor will prevent rebinding to the immobilized ligand. A significantly faster dissociation was observed in the presence of the competitor (supplemental Fig. S13*B*), indicating that the system was mass-transport limited and that the true dissociation rate was probably greater than the observed rate. Based on these findings, we concluded that kinetic analyses were untrustworthy in this system, and therefore we limited our data analysis to derivations of binding affinity from equilibrium measurements, which are unaffected by mass-transport limitations.

Table S1. Expression constructs used in this work and primers used to generate them. Plasmids pETHSUL and pETCH have been described elsewhere (2). For all the His_6-SUMO-fusions, a single glycine residue was inserted between the protease cleavage site and the N-terminus of each protein, to increase the efficiency of cleavage by the SUMO-specific protease Ud1.

Target	**Primers (5′-3′)**	**Plasmid Backbone**	**Cloning Method**
p97	1: AGATTGGTGGCATGGCTTCTGGAGCCGATTCAAA 2: GAGGAGAGTTTAGACATTAGCCATACAGGTCATCATCATTG	pETHSUL	LIC
p97-1D4	1: AATGATGATGACCTGTATGGCACCGAAACCTCTCAGGTGGCGCC GGCGTAATGTCTAAACTCTCC 2: GGTGCCATACAGGTCATCATCATTGTCTTCTGTGTATACACTGCC ACCTGTGCCGC	pETHSUL	Insertion mutagenesis pETHSUL-p97 template
p97-His_6	1: TTTTTTTTTTTCTAGAATGTCTGACTCCGAAGTCAATCAAG 2: TTTTTTTTTTCCCGGGGCCATACAGGTCATCATCATTG	pETCH	Xba1/Xma1digestion and ligation
p97 N-domain	1: AGATTGGTGGCATGGCTTCTGGAGCCGATTCAAA 2: GAGGAGAGTTTAGACATTACTCCCCTTCGCAGTGGATCAC	pETHSUL	LIC
p97 ND1	1: AGATTGGTGGCATGGCTTCTGGAGCCGATTCAAA 2: GAGGAGAGTTTAGACATTACCCGATGTCTTCCCAGGTTAC	pETHSUL	LIC
Ataxin3	1: AGATTGGTGGCGGTATGGAGTCCATCTTCCACGAG 2: GAGGAGAGTTTAGACTATTATTTTGGTCGATGCATCTGTTGG	pETHSUL	LIC
His_6-Ataxin3	1: TTTTTTTTTTTCCATGGGTATGGAGTCCATCTTCCACG 2: TTTTTTTTTTGCGGCCGCGACTAGTGAGCTCG	pProEX-HTb	Nco1/Not1 digestion and ligation
Ataxin3 Josephin domain	1: AGATTGGTGGCGGTATGGAGTCCATCTTCCACGAG 2: GAGGAGAGTTTAGACTATTATTTTGGTGTATCCATCTCTTCGA	pETHSUL	LIC
Ataxin3 Josephin+UIMs	1: AGATTGGTGGCGGTATGGAGTCCATCTTCCACGAG 2: GAGGAGAGTTTAGACATTAGTTTCTGGAACTACCTTGCATA CTTAG	pETHSUL	LIC
Ataxin3ΔC	1: GAGAAGCAATAATCAGCAGCAACAACAACAACAGCAACAACAG CGGGACC 2: TGCTGCTGATTATTGCTTCTCAAAGTAGGCTTCTCGTCTCTTCCGA AGC	pETHSUL	Insertion mutagenesis pETHSUL-ataxin3 template
Ataxin3ΔN	1: AGATTGGTGGCGGAATGTTAGACGAAGATGAGGAGG 2: GAGGAGAGTTTAGACTATTATGTCAGATAAAGTGTGAAGGT	pETHSUL	LIC

Abbreviations: Ligation independent cloning (LIC), p97 N- and D1- domains (p97 ND1) and Ubiquitin interacting motifs (UIMs).

Table S2. Primers used for one-step site-directed mutagenesis of ataxin3 and p97 (7). pETHSUL-ataxin3 and pETHSUL-p97-1D4 were used as templates.

Ataxin3 mutant construct	**Primers (5′-3′)**
^{282}ANAA^{285}	1: GAGCTTGCGAACGCGGCGGAAGCCTACTTTGAGAAGCAACAGCAGCAAC 2: AAAGTAGGCTTCCGCCGCGTTCGCAAGCTCTTCTGAAGTAAGATTTGTACCTG
p97 mutant construct	**Primers (5′-3′)**
Y143A	1: CTGGAAGCGGCTCGACCCATCCGGAAAGGAGACATTTTTCTTGTCCG 2: GGTCGAGCCGCTTCCAGGAAGTACGGCTTAAGGTATACCTCGAAGAG
L72A	1: CATCGTCGCTTCTGATGATACTTGTTCTGATGAGAAGATTCGGATGAATAGAG 2: CATCAGAAGCGACGATGCAAACAGCTTCTCGTCTCTTCTTTCCTTTCAGC
R53A	1: GTTGTTCGCAGGTGACACAGTGTTGCTGAAAGGAAAGAAGAGACGAGAAGCTG 2: GTGTCACCTGCGAACAACTGCAATTCATCCATCTTGGGCTGGGACAAG
G54W	1: GTTCCGATGGGACACAGTGTTGCTGAAAGGAAAGAAGAGACGAGAAG 2: CTGTGTCCCATCGGAACAACTGCAATTCATCCATCTTGGGCTGGG
K251A	1: GAACAGGAGCTACCCTGATTGCTCGAGCTGTAGCAAATGAGACTGGAG 2: ATCAGGGTAGCTCCTGTTCCAGGAGGTCCGTAAAGCAGGATTCCTC
K524A	1: CTGTGGGGCTACTTTGTTGGCCAAAGCCATTGCTAATGAATGCCAG 2: CAACAAAGTAGCCCCACAGCCAGGAGGTCCATAGAACAGAACTCCC
K251A/K524A	K251A and K524A were used together
R155C/N387C	R155C 1: TTTTCTTGTCTGCGGTGGGATGCGTGCTGTGGAGTTCAAAGTGGTGG 2: CCACCGCAGACAAGAAAAATGTCTCCTTTCCGGATGGGTCGATACG N387C 1: AAGTGCATGAAGCTGGCAGATGATGTGGACCTGGAACAGGTAGCCAATG 2: CTGCCAGCTTCATGCACTTGGTATGGATCTGAAGAATCTCTAAGCGTCC
R155H	1: TTTTCTTGTCCATGGTGGGATGCGTGCTGTGGAGTTCAAAGTGGTGG 2: CCACCATGGACAAGAAAAATGTCTCCTTTCCGGATGGGTCGATACG
L198W	1: AGAGTCCTGGAATGAAGTAGGGTATGATGACATTGGTGGCTGCAGG 2: ACTTCATTCCAGGACTCTTCCTCATCCTCTCGTTTGATAGGCTCCC
A232E	1: CCCTCTTTAAGGAAATTGGTGTGAAGCCTCCTAGAGGAATCCTGC 2: CCAATTTCCTTAAAGAGGGCAGGATGTCTCAGGGGCAGTTCCAC
L198W/R155C/N387C	L198W primers were used with the pETHSUL-R155C/N387C mutant
A232E/R155C/N387C	A232E primers were used with the pETHSUL-R155C/N387C mutant

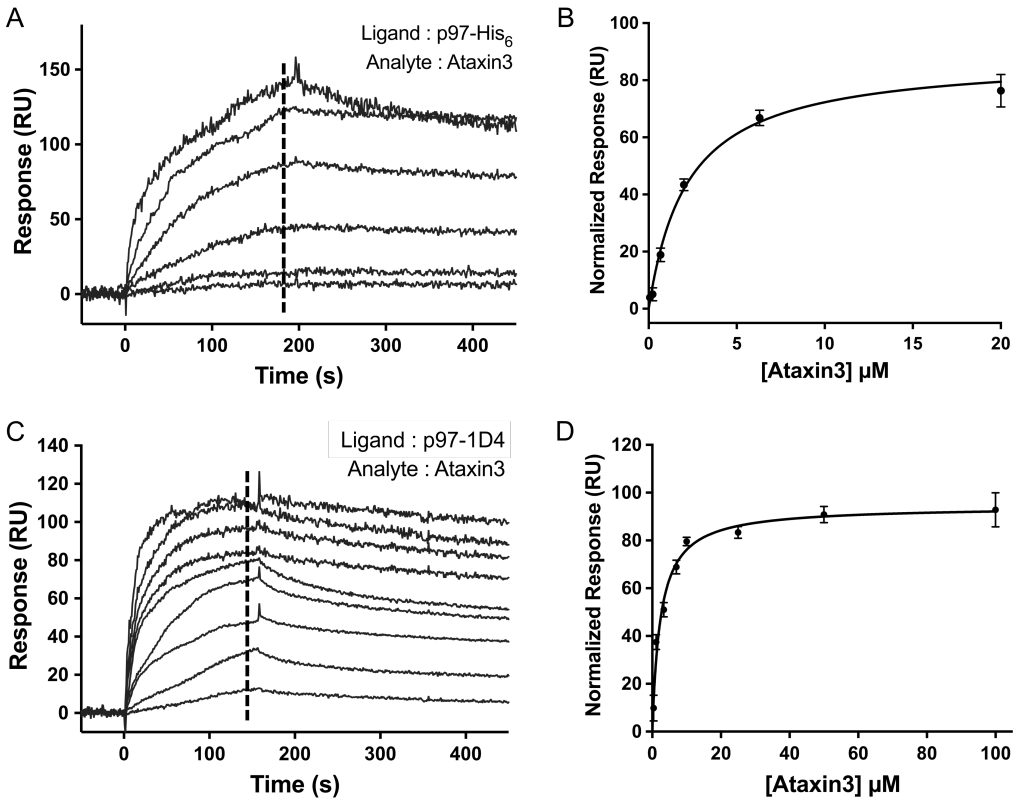

Figure S1. Alternate p97 preparations have the same affinity for ataxin3. **(A)** Representative sensorgram for full-length ataxin3 binding to full-length p97-His_6 (ataxin3 concentrations 0–20 µM, $n \geq 3$ for each concentration). **(B)** Normalized equilibrium response fit of the data in A to a one-site binding curve (K_D = 2.2 ± 0.2 µM). **(C)** Representative sensorgram for full-length ataxin3 binding to full-length p97-1D4 (ataxin3 concentrations 0–100 µM, n ≥ 3 for each concentration). The p97-1D4 sample was purified using an additional ion exchange chromatography step, similar to the ITC sample preparation. **(D)** Normalized equilibrium response fit of the data in C to a one-site binding curve (K_D = 2.4 ± 0.2 µM). The dashed lines in the left panels represent the response range used to determine the fit.

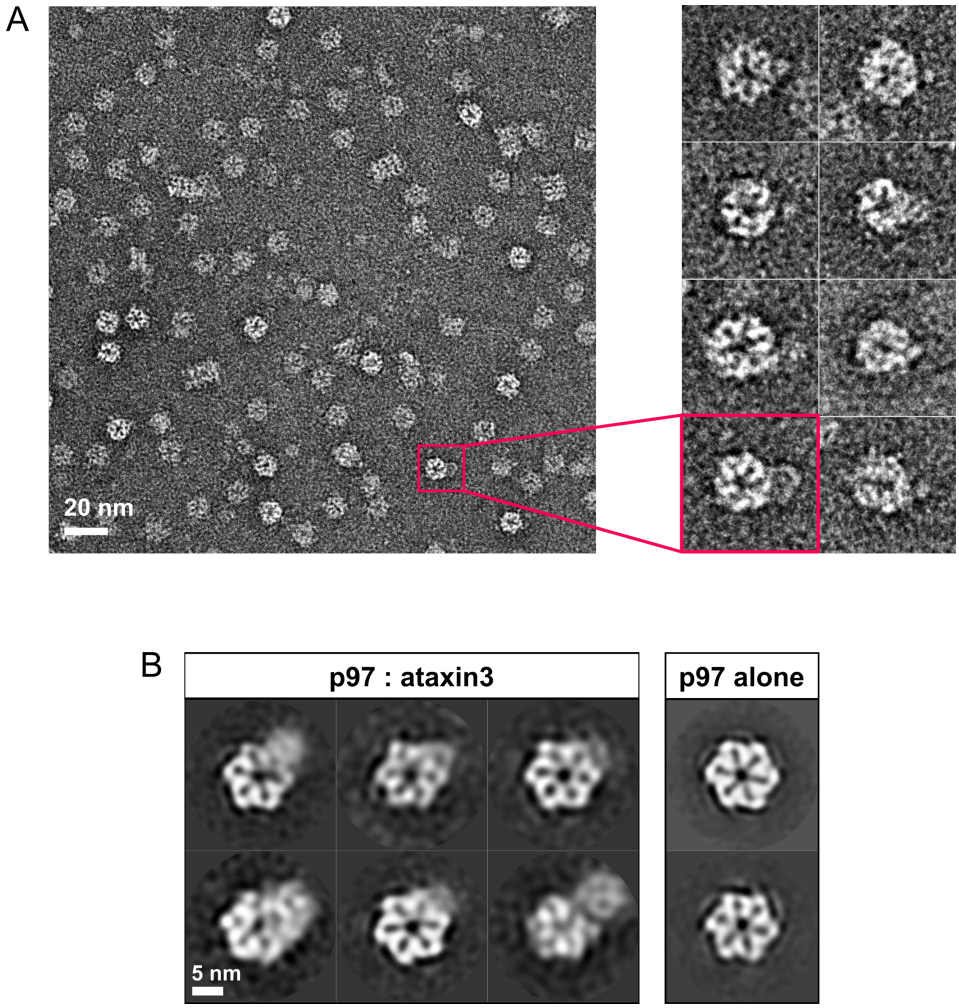

Figure S2. Negative-stain electron microscopy (EM) analyses of the p97-ataxin3 complex. **(A)** *Left*, electron micrograph showing negatively-stained hexamers of p97 bound to ataxin3 (non-crosslinked). The *magenta box* highlights one p97-ataxin3 complex. *Right,* raw images of the complex viewed down the 6-fold axis, shown at higher magnification. **(B)** Representative 2D class averages for the non-crosslinked p97-ataxin3 complex (*left*) and p97 alone (*right*). From the 20,256 particles selected, only ~1,300 particles were sorted into classes that show the additional blurred density corresponding to ataxin3. No side views of the p97 hexamer were observed in any samples, suggesting that the relatively flat, disk-shaped hexamer adopts a preferred orientation coplanar with the plane of the EM grid.

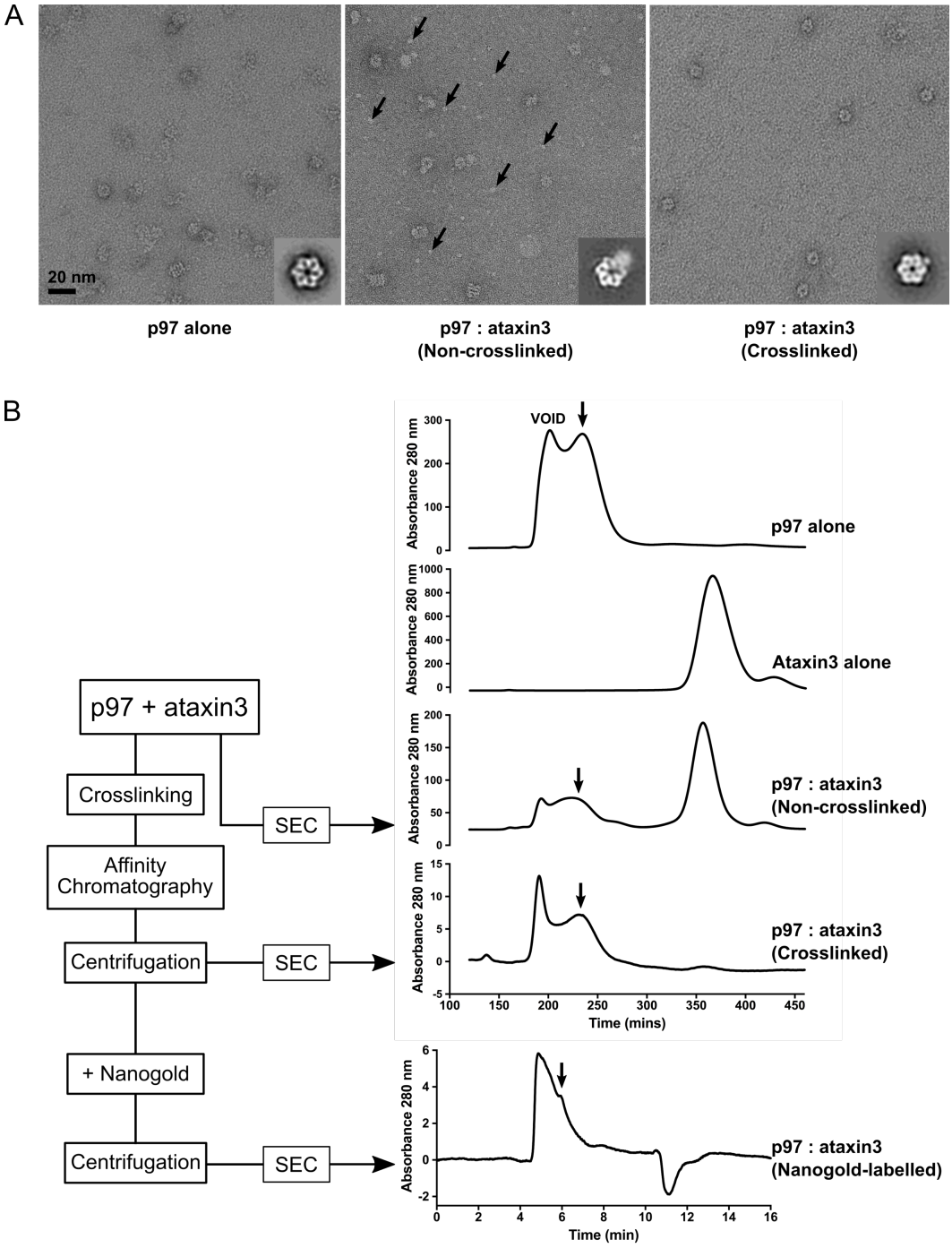

Figure S3. Comparison of non-crosslinked and crosslinked samples. **(A)** Negative-stained electron micrographs showing p97 alone, non-crosslinked p97-ataxin3 complexes, and crosslinked complexes. *Insets* show a representative 2D class average from each experiment. Note the presence of numerous particles in the middle micrograph (*black arrows*), of a size significantly smaller than the expected dimensions for p97; these particles are absent in the other two micrographs. These particles may represent free ataxin3, implying that the complex has dissociated either during the SEC step or during grid preparation. The blurred density seen for the non-crosslinked complexes might therefore reflect partial

dissociation, which is resolved by crosslinking. **(B)** Workflow for preparation of complexes for EM, along with SEC chromatograms for p97 alone, ataxin3 alone, and the non-crosslinked, crosslinked and Nanogold-labelled complexes. The *black arrows* indicate the fractions used for negative-stain EM. As seen from the position of the peaks, the complex peak may overlap with the p97-alone peak. In the non-crosslinked experiment, the inability to resolve these peaks may have introduced free p97 in the fraction applied to the grids, which would also account for the relatively low fraction of particles containing the complex (~5% of the total particles). The crosslinking, affinity purification, and centrifugation steps aided in removal of unbound p97 and ataxin3 (note the disappearance of the ataxin3 alone peak in the chromatogram for the crosslinked complex). The p97-alone chromatogram shows a typical purification profile similar to others described previously, with irreversibly aggregated material in the void volume peak (3). Note that a different SEC column was used for the Nanogold-labelled material as compared to the other complexes (see Methods), which explains the difference in elution times.

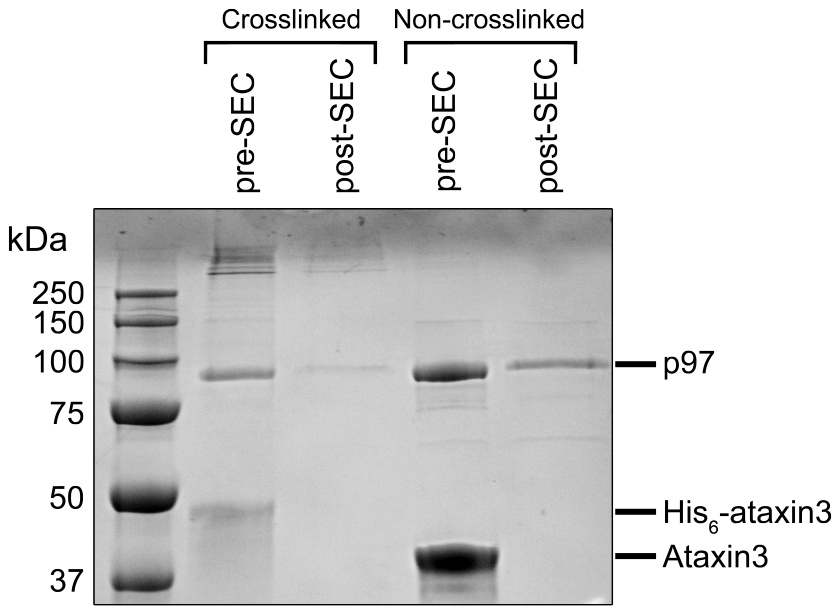

Figure S4. SDS-PAGE gel of the crosslinked and non-crosslinked EM complexes, stained with Coomassie Brilliant Blue. Lane 1 is the His_6-ataxin3-p97 complex crosslinked with 0.05% glutaraldehyde and purified by immobilized metal-affinity chromatography. Lane 2 is the crosslinked sample from lane 1 after SEC. Lanes 3 and 4 are the p97-ataxin3 complex without crosslinker before and after SEC respectively. In lanes 2 and 4, the tagged and untagged ataxin3 bands are not visible at the dilutions obtained after SEC.

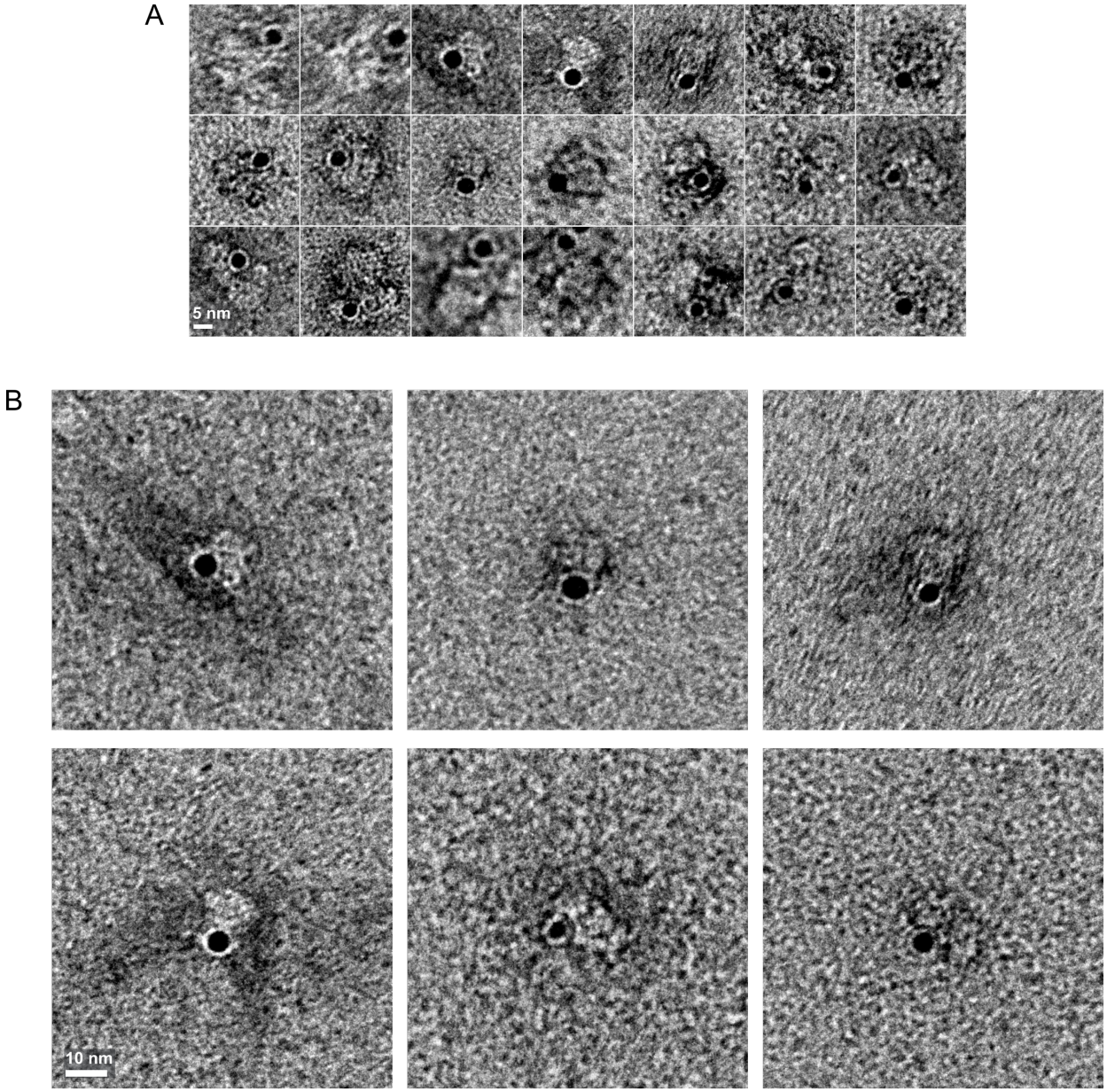

Figure S5. (A) Raw images of p97 complexed with Nanogold-labelled ataxin3. One single gold particle, visible as a black dot, is observed per complex. **(B)** Six additional complex images as above, shown at higher magnification.

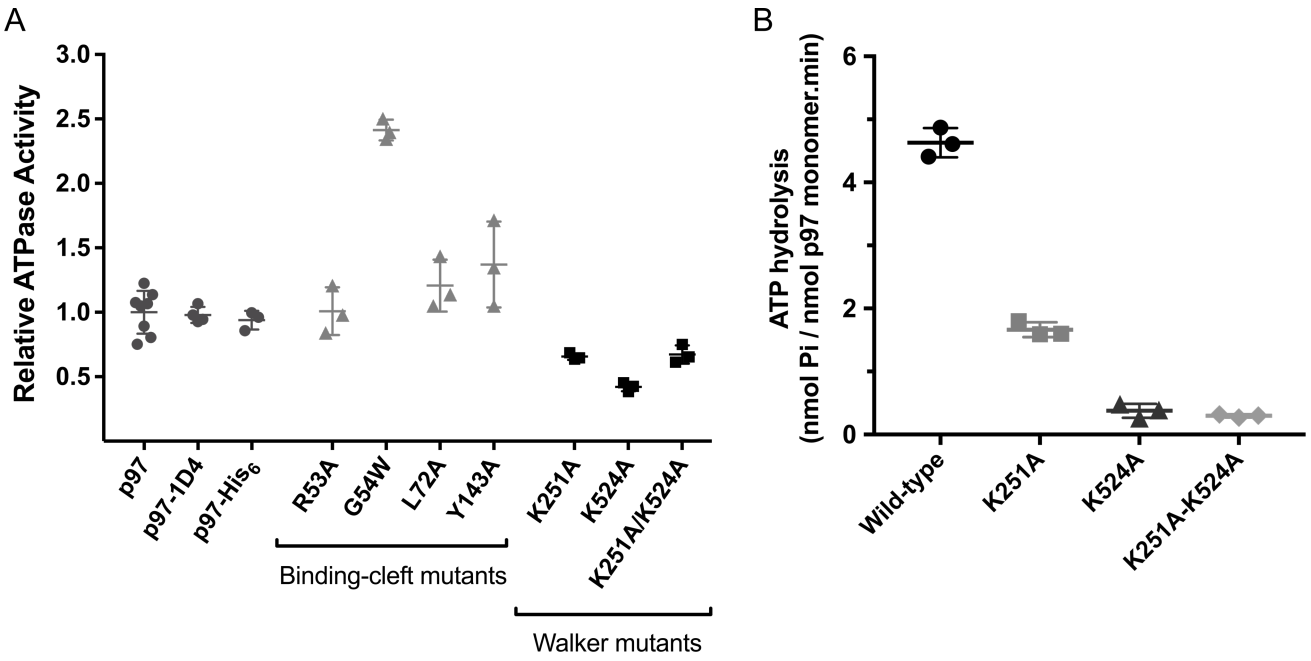

Figure S6. ATPase activities of wild-type and mutant p97. **(A)** ATPase activities of full-length wild-type p97 (untagged and tagged), four cofactor binding-cleft mutants, and three Walker mutants (all mutants are 1D4-tagged). The C-terminal 1D4 and His_6 tags do not affect ATP hydrolysis. G54W is not an identified MSP1 mutation and it is thus unclear why that mutant has elevated activity ($n \geq 3$ for all measurements). **(B)** We noticed that the relative activities of Walker mutants *vs.* wild-type p97, as shown in panel (A), do not follow the same trend as seen in Briggs *et al.* (8); specifically, in our hands, the K524A mutants appear to possess higher activity than previously reported. However, the activities cannot be directly compared, since different assay conditions were used. The experiments in panel (A) rely upon a coupled assay linked to NADH consumption and were performed at room temperature; in contrast, the Briggs *et al.* experiments utilize a colorimetric Malachite Green assay, performed at 37°. Therefore, to determine whether these disparities in relative activities reflect differences in the assay conditions or genuine differences in the proteins, we measured the ATPase activities of our p97 proteins using a Malachite Green assay at 37 °C, as described in (8). We found that under these conditions, the activities of our different p97 variants follow a trend that is very similar to previously published results (8,9), demonstrating that the apparent disparity in activities results from different assay conditions, and not from different behavior on the part of the proteins.

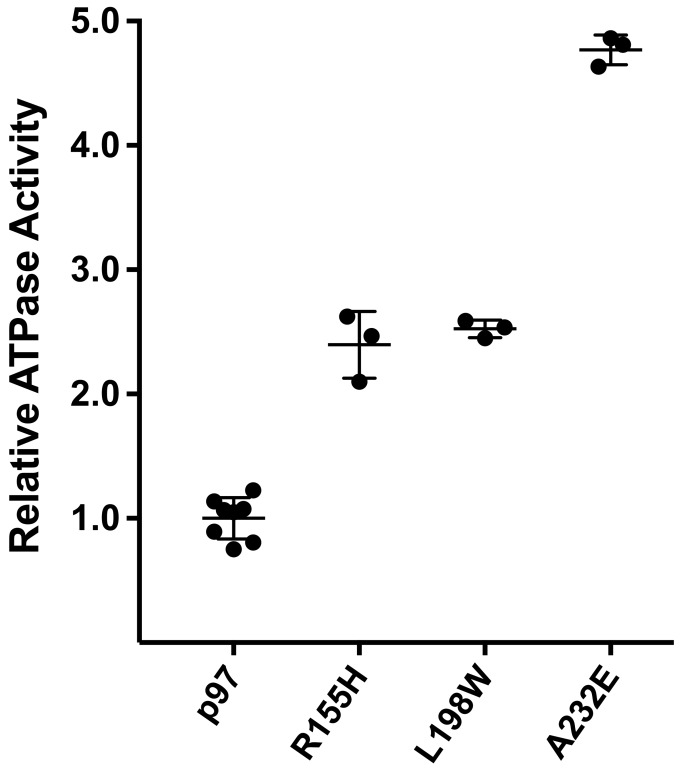

Figure S7. ATPase activities of full-length wild-type p97 and three MSP1 mutants. The mutants show increased activity as compared to the wild-type, consistent with previously published data (3,10).

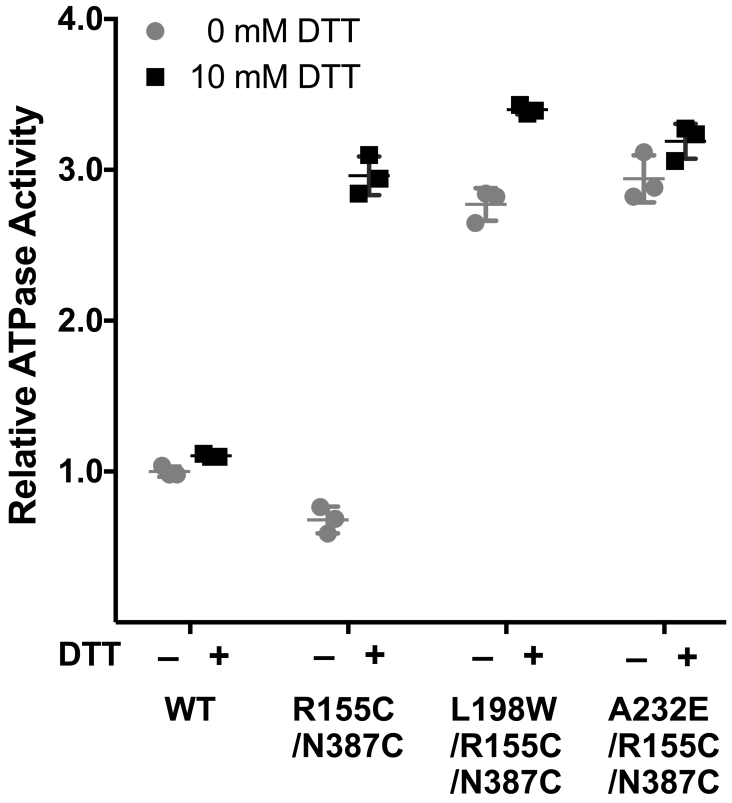

Figure S8. ATPase activities of full-length wild-type p97 (WT), the R155C/N387C double mutant, and the L198W and A232E MSP1 mutant versions of the R155C/N387C double mutant, all measured in the presence and absence of DTT. Note that the disulfide-locked form (– DTT) of the R155C/N387C double mutant has very low activity, which is rescued in the presence of reducing agent (+ DTT). The L198W and A232E versions of the R155C/N387C double mutant show no difference in activity with and without DTT. This suggests that in the two mutants, Cys-155 and Cys-387 are never in close enough proximity to form a disulfide bond and lock down the N-domain.

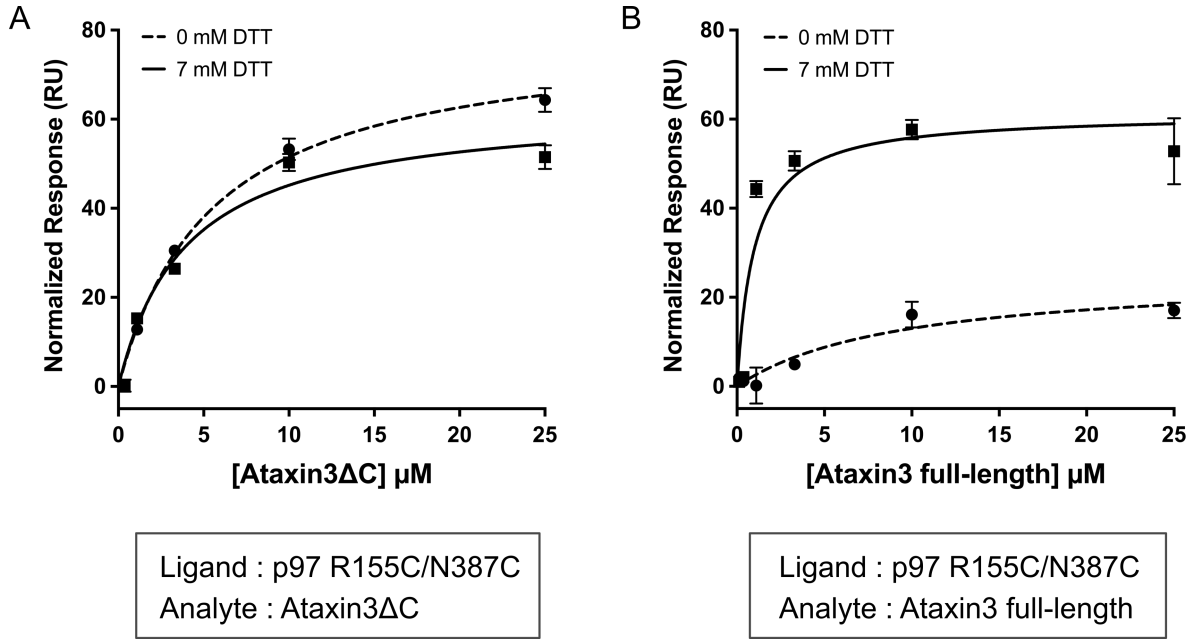

Figure S9. Ataxin3ΔC binds equally to the disulfide-locked form (– DTT) and reduced form (+ DTT) of the R155C/N387C p97 double mutant, unlike full-length ataxin3. Normalized equilibrium binding response for **(A)** ataxin3ΔC and **(B)** full-length ataxin3 binding to the R155C/N387C double mutant, in the presence and absence of 7 mM DTT ($n \geq 3$ at each concentration for both analytes). The data shown in (B) are the same as those shown in Fig. 7*B*.

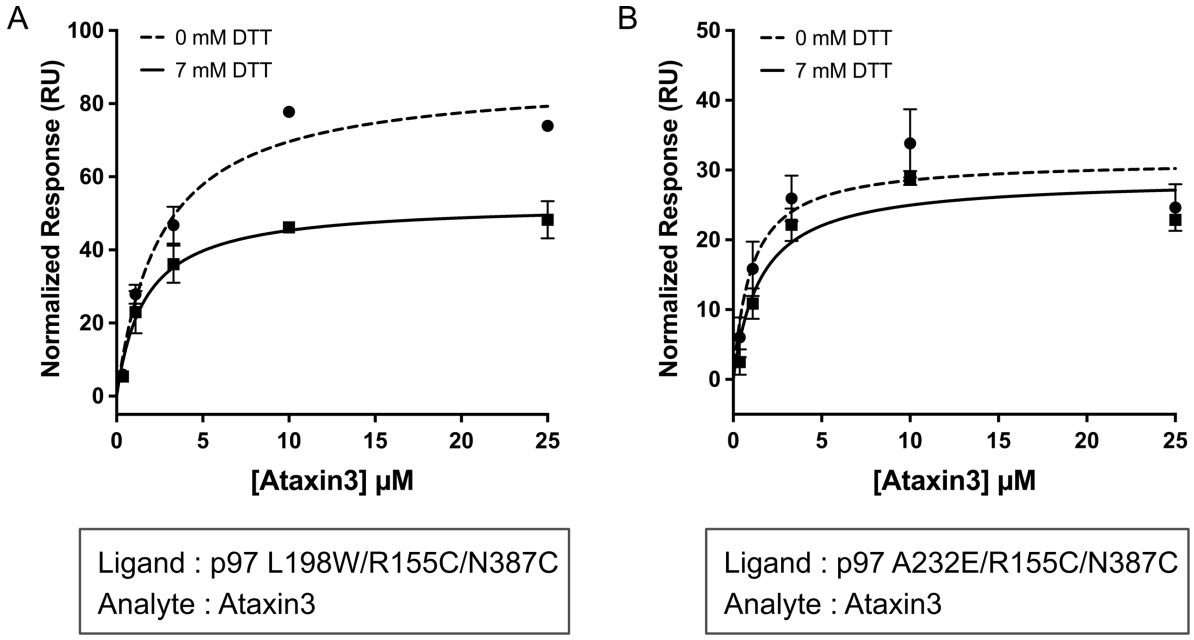

Figure S10. Ataxin3 binds the MSP1 mutant versions of the R155C/N387C double mutant, both in the presence and absence of DTT. Normalized equilibrium binding response for ataxin3 ($n \geq 3$ at each concentration) binding to the **(A)** L198W and **(B)** A232E versions of the R155C/N387C double mutant, with and without 7 mM DTT.

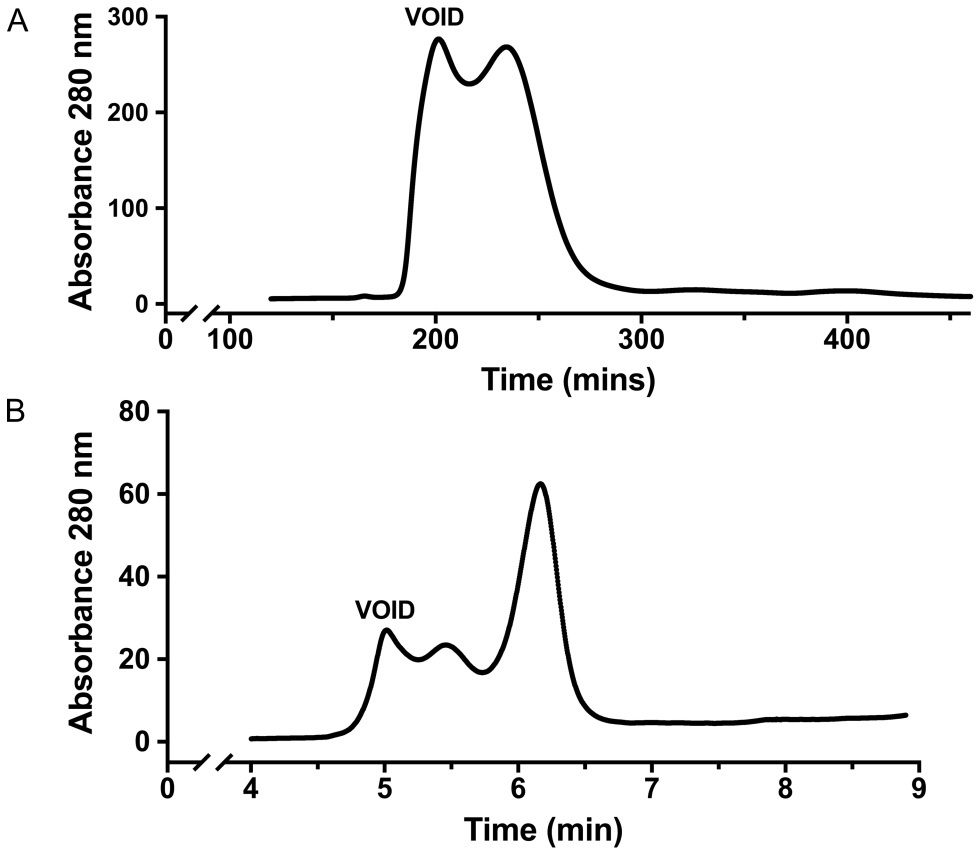

Figure S11. SEC elution profile of full-length p97 from the **(A)** Sephacryl S-300 preparative column and **(B)** Yarra SEC-3000 column. The void peak in both contains aggregated material. A smaller peak is resolved in (B), eluting between the void and hexamer peaks, and most likely contains higher-order oligomers such as dodecamers and/or small aggregates. The elution profile in (A) is the same as the p97-alone profile shown in Fig. S3*B*.

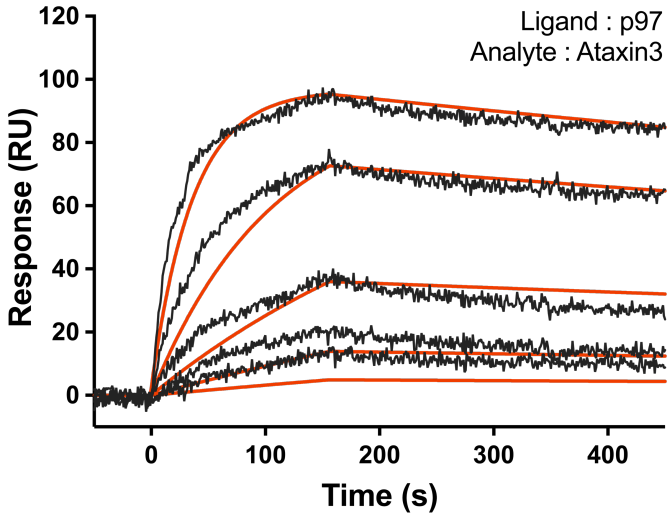

Figure S12. Representative SPR sensorgrams for the binding of full-length ataxin3 to full-length 1D4-tagged p97. Highest ataxin3 concentration = 10 μM; other concentrations obtained by successive 3-fold dilutions. The *orange lines* represent a global fit to a one-site kinetic model. Note that the fit deviates considerably from the sensorgrams, especially at the lower concentrations, and thus reliable kinetic rates cannot be derived. This could either be resolved by fitting to a more complex model or by accounting for surface-induced mass-transport limitations.

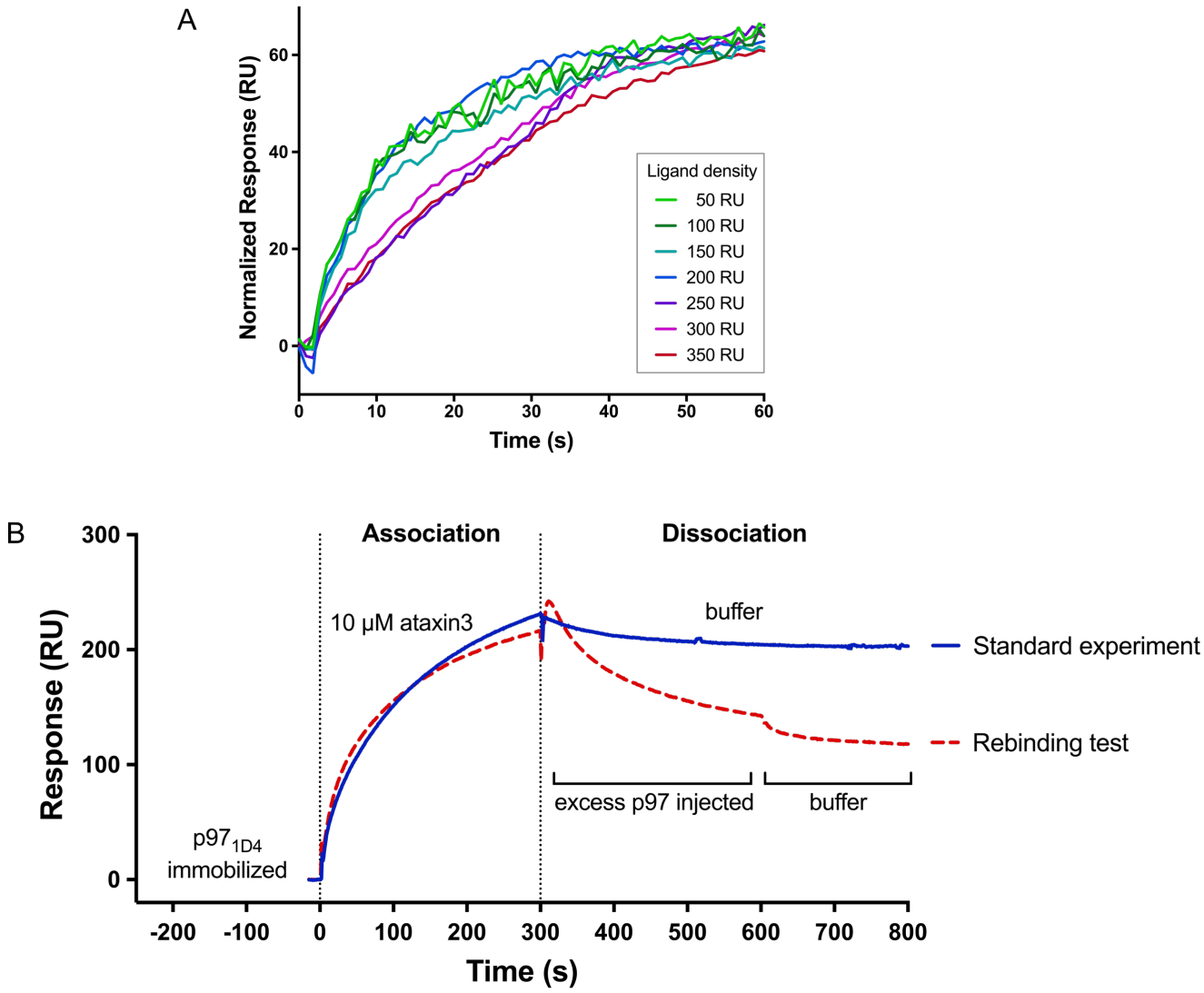

Figure S13. Detecting the presence of mass-transport limitations in the p97-ataxin3 system. **(A)** Comparison of the association signals from 10 μM ataxin3 binding to different densities (50–350 RU) of the immobilized ligand p97-1D4. The responses are normalized to the density of p97-1D4 on each corresponding surface. Superimposable responses were obtained for surfaces with densities between 50–200 RU; ligand densities greater than 200 RU showed slower association, indicating the presence of mass-transport effects. **(B)** Data showing the association and dissociation between 10 μM ataxin3 analyte and p97-1D4 ligand, obtained under standard experimental conditions *(blue line),* and rebinding test conditions *(dashed red line)*. Rebinding was tested by injecting excess untagged p97 during the dissociation phase (instead of the running buffer alone); the excess p97 serves as a competitor and binds the dissociated ataxin3, preventing its rebinding to the immobilized p97-1D4. Note the significantly faster dissociation under these conditions, indicating that analyte rebinding is occurring under the standard experimental conditions, implying that the true dissociation rate is probably greater than that observed in the standard experiment.

Table S3. Binding affinities and structures for various p97-cofactor complexes.

p97 construct	Cofactor construct	K_D	Technique	p97-interacting domain/motif	PDB entry for the complex	References
N	Ufd1 peptide	221 μM	ITC	SHP box	5B6C	(11)
N	Npl4 ULD	17.8 μM	ITC	ULD	2PJH	(12,13)
FL p97	FL Ufd1/Npl4	1.7 μM	ITC	SHP box / ULD		(14)
ND1	FL Ufd1/Npl4	2.1 μM	ITC			
FL p97	FL Otu1	0.71 μM	ITC	UBXL	4KDI, 4KDL	(15)
FL p97	FL p47	0.7 μM	ITC	UBX / SHP box	1S3S	(14,16,17)
ND1	FL p47	0.54 μM	ITC			
FL p97	FL p47	22 nM, 0.89 μM	SPR			
FL p97	FL p37	19 nM	SPR	UBX		(17)
ND1	Faf1 UBX	30 μM	ITC	UBX	3QQ8, 3QWZ	(12,14)
N	Faf1 UBX	25.6 μM	ITC			
ND1	FL SVIP	0.67 μM	ITC	VIM		(18,19)
NL	FL SVIP	5.92 μM	ITC			
N	SVIP peptide	6.6 μM	ITC			
ND1	gp78 peptide	21.3 nM	BLI	VIM	3TIW	(18,19)
N	gp78 peptide	5 μM	ITC			
ND1	ANKZF1 peptide	16.3 nM	BLI	VIM		(18)
FL p97	FL UBXD1	3.5 μM	ITC	VIM / PUB		(18)
N	RHBL4 C-terminal	68.9 μM	SPR	VBM	5EPP	(20)
N	Hrd1 peptide	47.8 μM	ITC	VBM		(19)
N	E4B peptide	46.3 μM	ITC	VBM		(19)
N	Ataxin3 peptide	15.6 μM	ITC	VBM		(19) and this study
FL p97	FL Ataxin3	3.7 ± 0.9 μM	SPR			
N	FL Ataxin3	6.4 ± 1.5 μM	SPR			
N	FL Ataxin3	4.5 ± 0.2 μM	ITC			

Abbreviations: Full-length (FL), p97 N- and D1- domains (ND1), p97 N-domain (N), Ubiquitin-fusion degradation protein 1 (Ufd1), Nuclear localization protein 4 (Npl4), Ovarian tumor domain-containing protein 1 (Otu1), Fas-associated factor 1 (Faf1), Small valosin-interacting protein (SVIP), Ankyrin repeat and zinc finger domain-containing protein 1 (ANKZF1), Ubiquitin regulatory X domain protein 1 (UBXD1), Rhomboid protease (RHBDL4), HMG-CoA reductase degradation protein 1 (Hrd1), Isothermal Titration Calorimetry (ITC), Surface plasmon resonance (SPR), Biolayer interferometry (BLI), Ubiquitin-like domain (ULD, also known as UBD), Ubiquitin regulatory X domain (UBX), UBX-like domain (UBL), peptide:N-glycanase/ UBA or UBX (PUB), p97/VCP-interacting motif (VIM), and p97/VCP-binding motif (VBM).

REFERENCES

1. Studier, F. W. (2005) Protein production by auto-induction in high density shaking cultures. *Protein expression and purification* **41**, 207-234.
2. Weeks, S. D., Drinker, M., and Loll, P. J. (2007) Ligation independent cloning vectors for expression of SUMO fusions. *Protein expression and purification* **53**, 40-50.
3. Niwa, H., Ewens, C. A., Tsang, C., Yeung, H. O., Zhang, X., and Freemont, P. S. (2012) The role of the N-domain in the ATPase activity of the mammalian AAA ATPase p97/VCP. *The Journal of biological chemistry* **287**, 8561-8570.
4. Molday, L. L., and Molday, R. S. (2014) 1D4: a versatile epitope tag for the purification and characterization of expressed membrane and soluble proteins. *Methods in molecular biology (Clifton, N.J.)* **1177**, 1-15.
5. Locatelli-Hoops, S. C., Gorshkova, I., Gawrisch, K., and Yeliseev, A. A. (2013) Expression, surface immobilization, and characterization of functional recombinant cannabinoid receptor CB2. *Biochimica et biophysica acta* **1834**, 2045-2056.
6. Schuck, P., and Zhao, H. (2010) The role of mass transport limitation and surface heterogeneity in the biophysical characterization of macromolecular binding processes by SPR biosensing. *Methods in molecular biology (Clifton, N.J.)* **627**, 15-54.
7. Zheng, L., Baumann, U., and Reymond, J. L. (2004) An efficient one-step site-directed and site-saturation mutagenesis protocol. *Nucleic acids research* **32**, e115.
8. Briggs, L. C., Baldwin, G. S., Miyata, N., Kondo, H., Zhang, X., and Freemont, P. S. (2008) Analysis of nucleotide binding to P97 reveals the properties of a tandem AAA hexameric ATPase. *The Journal of biological chemistry* **283**, 13745-13752.
9. Chou, T. F., Bulfer, S. L., Weihl, C. C., Li, K., Lis, L. G., Walters, M. A., Schoenen, F. J., Lin, H. J., Deshaies, R. J., and Arkin, M. R. (2014) Specific inhibition of p97/VCP ATPase and kinetic analysis demonstrate interaction between D1 and D2 ATPase domains. *Journal of molecular biology* **426**, 2886-2899.
10. Zhang, X., Gui, L., Zhang, X., Bulfer, S. L., Sanghez, V., Wong, D. E., Lee, Y., Lehmann, L., Lee, J. S., Shih, P. Y., Lin, H. J., Iacovino, M., Weihl, C. C., Arkin, M. R., Wang, Y., and Chou, T. F. (2015) Altered cofactor regulation with disease-associated p97/VCP mutations. *Proceedings of the National Academy of Sciences of the United States of America* **112**, E1705-1714.
11. Le, L. T., Kang, W., Kim, J. Y., Le, O. T., Lee, S. Y., and Yang, J. K. (2016) Structural Details of Ufd1 Binding to p97 and Their Functional Implications in ER-Associated Degradation. *PloS one* **11**, e0163394.
12. Lee, J. J., Park, J. K., Jeong, J., Jeon, H., Yoon, J. B., Kim, E. E., and Lee, K. J. (2013) Complex of Fas-associated factor 1 (FAF1) with valosin-containing protein (VCP)-Npl4-Ufd1 and polyubiquitinated proteins promotes endoplasmic reticulum-associated degradation (ERAD). *The Journal of biological chemistry* **288**, 6998-7011.
13. Isaacson, R. L., Pye, V. E., Simpson, P., Meyer, H. H., Zhang, X., Freemont, P. S., and Matthews, S. (2007) Detailed structural insights into the p97-Npl4-Ufd1 interface. *The Journal of biological chemistry* **282**, 21361-21369.
14. Hanzelmann, P., Buchberger, A., and Schindelin, H. (2011) Hierarchical binding of cofactors to the AAA ATPase p97. *Structure (London, England : 1993)* **19**, 833-843.
15. Kim, S. J., Cho, J., Song, E. J., Kim, S. J., Kim, H. M., Lee, K. E., Suh, S. W., and Kim, E. E. (2014) Structural basis for ovarian tumor domain-containing protein 1 (OTU1) binding to p97/valosin-containing protein (VCP). *The Journal of biological chemistry* **289**, 12264-12274.
16. Dreveny, I., Kondo, H., Uchiyama, K., Shaw, A., Zhang, X., and Freemont, P. S. (2004) Structural basis of the interaction between the AAA ATPase p97/VCP and its adaptor protein p47. *The EMBO journal* **23**, 1030-1039.
17. Bulfer, S. L., Chou, T. F., and Arkin, M. R. (2016) p97 Disease Mutations Modulate Nucleotide-Induced Conformation to Alter Protein-Protein Interactions. *ACS chemical biology* **11**, 2112-2116.
18. Hanzelmann, P., and Schindelin, H. (2011) The structural and functional basis of the p97/valosin-containing protein (VCP)-interacting motif (VIM): mutually exclusive binding of cofactors to the N-terminal domain of p97. *The Journal of biological chemistry* **286**, 38679-38690.
19. Liu, S., Fu, Q. S., Zhao, J., and Hu, H. Y. (2013) Structural and mechanistic insights into the arginine/lysine-rich peptide motifs that interact with P97/VCP. *Biochimica et biophysica acta* **1834**, 2672-2678.
20. Lim, J. J., Lee, Y., Ly, T. T., Kang, J. Y., Lee, J. G., An, J. Y., Youn, H. S., Park, K. R., Kim, T. G., Yang, J. K., Jun, Y., and Eom, S. H. (2016) Structural insights into the interaction of p97 N-terminus domain and VBM in rhomboid protease, RHBDL4. *The Biochemical journal* **473**, 2863-2880.